Biochimica et Biophysica Acta 1840 (2014) 120–128

Contents lists available at ScienceDirect

Biochimica et Biophysica Acta

journal homepage: www.elsevier.com/locate/bbagen

Identification and active site analysis of the 1-aminocyclopropane-1-carboxylic acid oxidase catalysing the synthesis of ethylene in *Agaricus bisporus*

Demei Meng [a], Lin Shen [a,*], Rui Yang [a], Xinhua Zhang [c], Jiping Sheng [b,*]

[a] College of Food Science and Nutritional Engineering, China Agricultural University, Beijing 100083, China
[b] School of Agricultural Economics and Rural Development, Renmin University of China, Beijing 100872, China
[c] School of Agriculture and Food Engineering, Shandong University of Technology, Zibo 255049, Shandong, China

ARTICLE INFO

Article history:
Received 14 April 2013
Received in revised form 27 August 2013
Accepted 28 August 2013
Available online 6 September 2013

Keywords:
Ethylene
Agaricus bisporus (J.E. Lange) Imbach
Mushroom
1-Aminocyclopropane-1-carboxylate oxidase (ACO)
Ethylene forming enzyme
Active site

ABSTRACT

Background: 1-Aminocyclopropane-1-carboxylate oxidase (ACO) is a key enzyme that catalyses the final step in the biosynthesis of the plant hormone ethylene. Recently, the first ACO homologue gene was isolated in *Agaricus bisporus*, whereas information concerning the nature of the ethylene-forming activity of this mushroom ACO is currently lacking.
Methods: Recombinant ACO from *A. bisporus* (Ab-ACO) was purified and characterised for the first time. Molecular modelling combined with site-directed mutagenesis and kinetic and spectral analysis were used to investigate the property of Ab-ACO.
Results: Ab-ACO has eight amino acid residues that are conserved in the Fe (II) ascorbate family of dioxygenases, including four catalytic residues in the active site, but Ab-ACO lacks a key residue, S289. In comparison to plant ACOs, Ab-ACO requires ACC and Fe (II) but does not require ascorbate. In addition, Ab-ACO had relatively low activity and was completely dependent on bicarbonate, which could be ascribed to the replacement of S289 by G289. Moreover, the ferrous ion could induce a change in the tertiary, but not the secondary, structure of Ab-ACO.
Conclusions: These results provide crucial experimental support for the ability of Ab-ACO to catalyse ethylene formation in a similar manner to that of plant ACOs, but there are differences between the biochemical and catalytic characteristics of Ab-ACO and plant ACOs.
General significance: This work enhances the understanding of the ethylene biosynthesis pathways in fungi and could promote profound physiological research of the role of ethylene in the regulation of mushroom growth and development.

1. Introduction

Ethylene is a potent gaseous hormone that controls many processes associated with plant growth and development, including germination, fruit ripening, senescence and responses to several stresses [1]. Ethylene is biologically active in trace amounts, and the effects of this hormone are commercially important [1]. Interestingly, ethylene is produced not only by plants but also by microorganisms [2–4]. In higher plants, ethylene is produced via two committed enzyme-catalysed steps from S-adenosyl-L-methionine (SAM), which involves 1-aminocyclopropane-1-carboxylic acid (ACC) as a key metabolic intermediate. Firstly, ACC synthase (ACS) catalyses the cyclisation of SAM into ACC, and subsequently ACC oxidase (ACO) catalyses the oxidative conversion of ACC to ethylene [1,5]. ACS and ACO are the two key enzymes of the ethylene biosynthetic pathway [6]. However, microbial ethylene biosynthesis occurs via two distinct pathways. Most microorganisms produce ethylene from methionine via 2-keto-4-methyl-thiobutyric acid by an NADH:Fe(III)EDTA oxidoreductase [7], and a few microorganisms efficiently produce ethylene from 2-oxoglutarate by an ethylene-forming enzyme (EFE) [8,9]. Moreover, the biosynthesis and utilisation of ACC are of rare occurrence in microorganisms, except in the slime mould *Dictyostelium mucoroides* [10] and *Penicillium citrinum* [11]. Though ACS was purified and characterised from the latter, ACC is converted to α-ketobutyrate and ammonia by the action of ACC deaminase instead of being oxidised to form ethylene by ACO [11]. These findings imply different ACC functions and ethylene synthesis pathways in microorganisms.

Abbreviations: ACC, 1-aminocyclopropane-1-carboxylic acid; ACO, ACC oxidase; Ab-ACO, *Agaricus bisporus* (J.E. Lange) Imbach ACC oxidase; SAM, S-adenosyl-L-methionine; ACS, ACC synthase; EFE, ethylene-forming enzyme; PCR, polymerase chain reaction; IPTG, β-D-thiogalactoside; MOPS, 3-(N-morpholino) propanesulphonic acid; DTT, dithiothreitol; PMSF, phenylmethanesulphonyl fluoride; SDS-PAGE, sodium dodecyl sulphate polyacrylamide gel electrophoresis; IBs, inclusion bodies; 3D, three-dimensional; CD, circular dichroism; ANS, anthocyanidin synthase; K_m, Michaelis constant

* Corresponding authors. Tel.: +86 10 62738456; fax: +86 10 62736474.
E-mail addresses: shen5000@cau.edu.cn (L. Shen), shengping@ruc.edu.cn (J. Sheng).

0304-4165/$ – see front matter © 2013 Elsevier B.V. All rights reserved.
http://dx.doi.org/10.1016/j.bbagen.2013.08.030

Agaricus bisporus (J.E. Lange) Imbach is a macro-fungus, which is a "medium-evolved" species between plants and microorganisms, that also produces ethylene during differentiation and development. A relationship between the sporocarp development and the appearance of the peaks of ethylene production has been investigated [12,13]. Nevertheless, neither evidence for a similar regulatory role of ethylene as in higher plants nor information on the route of ethylene biosynthesis has been found in *A. bisporus*. A homologous gene encoding ACO was recently isolated from *A. bisporus* during the genome project [14]. However, definite information on the nature of catalysing the production of ethylene in *A. bisporus* by Ab-ACO, which could regulate growth and development, is currently lacking.

By contrast, plant ACC oxidase has been scrutinised to various degrees. ACO is a member of a superfamily of oxygenases and oxidases, most members of which couple the reaction of the oxidative decarboxylation of α-ketoglutarate (α-KG) to substrate oxidation [15]. ACO is unusual as the enzyme does not require α-KG as a cosubstrate but uses the cosubstrate ascorbate and the activator CO_2 instead [16,17]. ACO couples the two-electron oxidation of ACC and ascorbate to produce ethylene, HCN, CO_2, and dehydroascorbate, using a single non-heme Fe (II) ion and dioxygen [16,18]. The active site of ACO contains the conserved Fe (II) binding residues, namely, a 2His–1Asp facial triad and the putative co-substrate hydrogen-binding residues (RXS) [19]. Thus, it is of interest and of significant importance to know if ACO in *A. bisporus* (Ab-ACO) has similar biochemical and structural characteristics. It is unknown whether Ab-ACO has catalytic residues similar to plant ACOs.

To address this need, we purified and analysed the biochemical properties of recombinant Ab-ACO. The residues that are involved in catalysis were identified by site-directed mutagenesis guided by protein structure homology modelling in combination with spectral analysis to identify the reported Ab-ACO as the ethylene-forming enzyme in *A. bisporus*.

2. Materials and methods

2.1. Cloning and expression of Ab-ACO proteins

Total RNA was isolated from the fruiting bodies of *A. bisporus* according to our optimised method [20] and was then stored at −80 °C for further use. First strand cDNA was synthesised using oligo-dT18 (Promega) and 2 μg total RNA treated with RNase-free DNase I and M-MLV reverse transcriptase (Promega), according to the method of Zhao et al. [21]. The coding sequence of ACO from *A. bisporus* was amplified from the first strand cDNA with EasyPfu DNA Polymerase (TransGen Biotech, Beijing, China) and specific primers, WT_for and WT_rev (Table 1), which were designed based on the genome sequence results of *A. bisporus var bisporus* v2.0 (URL, http://genome.jgi.doe.gov/Agabi_varbur_1). The resulting PCR product was ligated and introduced into the pET3a (Novagen Inc., Madison, WI, USA) expression plasmid, which contains an isopropyl β-D-thiogalactoside-inducible promoter and was used to express wild-type recombinant Ab-ACO.

2.2. Preparation of wild-type and mutant Ab-ACO proteins

Both wild-type and mutant plasmids were transformed into *Escherichia coli* BL21 (DE3) pLysS competent cells using conventional methods. The transformed *E. coli* cells were grown in Luria–Bertani broth with 50 μg/mL ampicillin, initially at 37 °C until the cultures reached in logarithmic phase ($OD_{600} \approx 0.5$). Thereafter, the cells were cooled to 27 °C to induce protein production by the addition of isopropyl-β-D-thiogalactoside (IPTG) at a final concentration of 0.5 mM. Induction was carried out at 27 °C for 8 h.

The cell pellets were harvested by centrifugation and were resuspended in a buffer containing 50 mM MOPS (3-(N-morpholino) propanesulphonic acid, pH 7.4), 1 mM dithiothreitol (DTT), 3 mM ascorbic acid, 10% (v/v) glycerol and 0.5% Triton X-100. For cell lysis, the suspension was sonicated on ice after 1 mM protease inhibitor phenylmethanesulphonyl fluoride (PMSF) was added. The soluble and insoluble fractions were separated by centrifugation at 10,000 *g* for 10 min at 4 °C. The pellet containing the insoluble recombinant pET3a-AbACO protein (inclusion bodies, IBs) was washed three times with 50 mM Tris–HCl (pH 8.0), 100 mM NaCl, 1 M urea, and 1% Triton X-100. Then, the pellet was resuspended in a buffer containing 8 M urea and 10 mM Tris–HCl (pH 7.4), and the pellet was then solubilised for 4 h with stirring at room temperature. The solubilised inclusion body was centrifuged at 10,000 *g* for 15 min at 4 °C, and the supernatant was collected.

Table 1
Oligonucleotides used for cloning and expression of wild-type and mutant Ab-ACO proteins.

Proteins	Oligonucleotide sequence[a]
WT_for	5′-GGGAATTCCATATGACTATCATAACCCAGCCTCCCG-3′
WT_rev	5′-CGCGGATCCATTATAATGCCGAAGTAAAACACCG-3′
H216D_f	5′-CGGAGTCTGGTTGAAAGGAAATACTGACTT-3′
H216D_v	5′-TTCCTTTCAACCAGACTCCGCCGGATTTAT-3′
H216D/D218E_f	5′-GGTTGAAAGGAATACTGAGTTTATGACGC-3′
H216D/D218E_v	5′-CTCAGTATTTCCTTTCAACCAGACTCCGCC-3′
H273Q_f	5′-ACAAGCCGACAATCCAAAGAGTGCGCC-3′
H273Q_v	5′-TTGGATTGTCGGCTTGTAGTAGCCTCC-3′
H216D/D218E/H273Q_f	5′-ACAAGCCGACAATCCAAAGAGTGCGCC-3′
H216D/D218E/H273Q_v	5′-TTGGATTGTCGGCTTGTAGTAGCCTCC-3′
R287G_f	5′-CCAACAAAACAAGACTGGAGTTGGACT-3′
R287G_v	5′-CAGTCTTGTTTTGTTGGTCCAGAGGTG-3′
G289S_f	5′-AACAAGACTAGAGTTAGTCTCTTATATTTC-3′
G289S_v	5′-ACTAACTCTAGTCTTGTTTTGTTGGTCCAG-3′

[a]Mutated nucleotides are shown in boldface and magenta.

Denatured proteins were refolded as described by Wang et al. [22] with minor modifications. The proteins were dialysed against 2 L of freshly made 6, 4, 2, 1.5, 1, 0.5, and 0 M urea, consecutively, with 50 mM Tris (pH 7.4), 12 mM Hepes (pH 7.4), 60 mM KCl, 1 mM EDTA and 1 mM DTT. For each concentration, the protein was dialysed for 12 h with stirring at 4 °C.

The wild-type and mutant Ab-ACO proteins were both purified according to the reported method [23]. The protein content was determined by the Bradford method with bovine serum albumin as standard [24]. SDS-PAGE was then performed to identify the proteins.

2.3. NH_2-terminal amino sequence analysis

The amino acid sequence of the N-terminus was determined using a Procise 491 protein sequencer (Applied Biosystems) by automated Edman degradation as described by Li et al. [25].

2.4. Sequence alignment and molecular modelling

To select candidates for site-directed mutagenesis, the amino acid sequence of ACO from *A. bisporus* was aligned with ACO1 from *Malus domestica* (SWISSPROT Q00985), ACO4 from *Solanum lycopersicum* (SWISSPROT P24157), ACO2 from *Carica papaya* (SWISSPROT Q9ZRC9), ACO1 from *Petunia hybrida* (SWISSPROT Q08506), ACO4 from *Arabidopsis thaliana* (SWISSPROT Q06588), and ACO4 from *Vigna radiata* (SWISSPROT Q2KTE3) using DNAMAN (5.2.2) and EMBOSS Needle (http://www.ebi.ac.uk/Tools/psa/) for multiply and pairwise sequence alignment, respectively.

The most successful general approach for predicting the structure of proteins involves the detection of homologs with known three-dimensional (3D) structure–template-based homology modelling or fold-recognition [26]; thus, several homologous proteins for the preliminary model of Ab-ACO were initially selected based on the GenTHREADER scores. However, all homologous proteins from the database showed <25% sequence identity. In general, alignment errors are relatively

high for proteins with <30% sequence similarity [27]. Therefore, the amino acid sequence of Ab-ACO was submitted to the Phyre^2 server (http://www.imperial.ac.uk/phyre/) [26] for remote homology/fold recognition to achieve high accuracy models at very low sequence identities (15–25%). The stereochemical qualities of the final model were evaluated by Procheck v3.5 [28] and Verify-3D [29] with the Swiss Model server (http://swissmodel.expasy.org) and the NIH MBI laboratory server (http://nihserver.mbi.ucla.edu), respectively.

2.5. Site-directed mutagenesis

Site-directed mutagenesis was performed using the Fast Mutagenesis System Kit (TransGen Biotech) according to the manufacturer's instructions. The pET3a plasmid with the *Ab-ACO* gene was used as a template for amplification of H216D, H216D/D218E, H273Q, R287G and G289S; and the H216D/D218E plasmid was used for H216D/D218E/H273Q amplification. The sequences of the sense/antisense mutagenic primer pairs are presented in Table 1. PCR stimulate was added during G289S plasmid amplification to optimise the template because of the low GC content (<35%) of the primer. Plasmids containing the correct mutation were identified by DNA sequencing.

2.6. Enzyme activity assay and kinetic analysis

The ACC oxidase activity assay was performed in sealed tubes as previously described, with some modifications [30]. The standard reaction 1.8 mL mixture comprised 100 mM Tris–HCl buffer (pH 7.2, containing 1.0 mM ACC, 30 mM ascorbic acid, 0.1 mM $FeSO_4$, and 30 mM $NaHCO_3$). Each of the enzyme kinetics was obtained by varying the concentration of one of the substrates while maintaining the concentration of the other substrates. The reaction was initiated by adding of 0.7 mL purified enzyme (0.084 mg/mL) and by sealing the tube with a rubber stopper. After incubation for 1 h at 30 °C with shaking, a 1 mL gas sample was withdrawn with a syringe from the head space of the sealed 10 mL tube for ethylene determination by a GC-4000A gas chromatograph (East & West Analytical Instruments, Inc., China) fitted with a flame ionisation detector. The column/injector/detector temperatures were set at 70, 120, 150 °C, respectively, and the carrier gas was N_2 with a flow rate of 30 mL/min. The results are the mean of three replicates. The K_m (Michaelis constant) of ACO was determined by measuring the reaction velocity at different substrate concentrations in a double reciprocal or Lineweaver–Burk plot.

2.7. Circular dichroism (CD) and fluorescence spectroscopy

Far-UV CD spectra were recorded on a PiStar-180 spectrometer (Applied Photophysics Ltd) under a constant flow of N_2 at 25 °C. The fluorescence emission spectra were scanned using a Cary Eclipse fluorescence spectrophotometer (Varian). The intrinsic Trp fluorescence of the protein was recorded by exciting the solution at 280 nm and measuring the emission in the 330–400 nm regions. All measurements were performed in 50 mM Tris–HCl buffer (pH 7.2), containing 0.15 mg/ml protein solution and the indicated concentration of $FeSO_4$ in triplicate.

3. Results

3.1. Cloning and preparation of recombinant Ab-ACO proteins

The coding sequence of *Ab-ACO* was amplified with specific primers based on the results of the *A. bisporus* genome project. The resulting RT-PCR product was 1104 bp long, and the recombinant Ab-ACO was expressed in *E. coli* with no degradation of the protein that was detected by SDS-PAGE. The supernatants and the pellets of the cell lysates were tested for the presence of recombinant proteins. As shown in Fig. S1, the majority of the expressed recombinant proteins were present in IBs that were insoluble and inactive protein aggregates [31]. This may be due to a protein translation rate that exceeds the cell capacity to fold the newly synthesised proteins [32]. However, IBs cannot be directly applied without solubilisation and refolding.

To isolate the Ab-ACO protein, the pellet was treated sequentially by disruption, washing and solubilisation to obtain an early pure denatured protein. Then, the protein was refolded and purified. The purified enzyme was >95% pure with an apparent estimated molecular weight of ~42 kDa (Fig. S1, lane 1), which was concurrent with the size of 42.03 kDa that was predicted by ProtParam (http://expasy.org/tools/protparam.html) analysis based on the amino acid sequence. The first 15 amino acids of the N-terminus of the purified Ab-ACO (MTIITQPPVVPHFVQ) were confirmed by Edman sequencing, and the purified recombinant enzyme was used for subsequent analysis.

3.2. Sequence alignment of the conserved Ab-ACO residues

The sequence alignment of ACO from *A. bisporus* with several plant species is presented in Fig. 1. The amino acid sequence of Ab-ACO exhibits very low (<25%) identity with plant ACOs and has 24 extra residues in the N-terminal region. However, Ab-ACO contains some conserved amino acid residues that are required for enzymatic activity, according to previous studies on recombinant plant ACOs. Specifically, eight of the twelve amino acid residues that are conserved among all members of a superfamily requiring Fe (II) and ascorbate for enzyme activities are present in Ab-ACO [33]. It is worth noting that the residues that have been proposed to be involved in the chelation of the Fe (II) ion (H216, H273 and D218) in the active site are also conserved in Ab-ACO [34]. Furthermore, F144, L166 and L173 that form the putative leucine zipper that is conserved in all known plant ACOs [35] are found in Ab-ACO. The leucine zipper with dimerisation potential may be involved in the binding of ACO to the membrane [35]. Although R287 which is required to bind with the ACC carboxyl group is conserved in Ab-ACO, S289 which forms a RXS motif with R287 is substituted by glycine. Importantly, the RXS motif is entirely conserved and regarded as a binding site for the carboxylate of ACC in plant ACOs [36].

3.3. Modelling structure and mutagenesis data

To gain a better understanding of the role of Ab-ACO in ethylene formation, 3D homology modelling (Fig. 2) was predicted by Phyre^2 to deduce the target residues for site-directed mutagenesis. The Ab-ACO model based on ANS structure (anthocyanidin synthase; PDB code 1GP6) exhibits good geometric and stereochemical quality, encompassing 343 residues (93% of the Ab-ACO sequence) with 100% confidence by the single highest scoring template. The Ramachandran plot (Fig. S2) and Verify3D scores (Fig. S3) indicate an acceptable model quality, showing over 99% of residues in the allowed regions and 82% of residues with 3D scores above 0.2.

Although ANS and Ab-ACO have only 18% sequence identity, the tertiary structures of these proteins are similar, particularly in the folding motif. The main chain of Ab-ACO contains ten α helices and thirteen β strands, of which seven (β5–11) form a β-jellyroll or double-stranded β helix topology (Fig. 2A, B). The jellyroll forms a hydrophobic cavity, one end of which forms the active site in a similar manner to the structure of ANS [37]. Four of the five strictly conserved amino acid residues (H216, H273, D218, R287) that are necessary for the activity of plant ACOs are in the hydrophobic cavity (Fig. 2B, C). Three residues (H216, H273 and D218), forming a facial catalytic triad, fold into a compact jelly-roll motif with a well-conserved Fe^{2+}-binding pocket, as seen in other dioxygenases of the same family (Fig. 2B, C). To confirm that the three residues were the Fe (II) binding ligands, each residue was systematically subjected to site-directed mutagenesis to generate variants for kinetic analysis and spectral studies. Interestingly, each mutation lowered the ACC oxidase activity, but mutants of H216D, H273Q and H216D/D218E still retained 76%, 62% and 78% of enzyme activity,

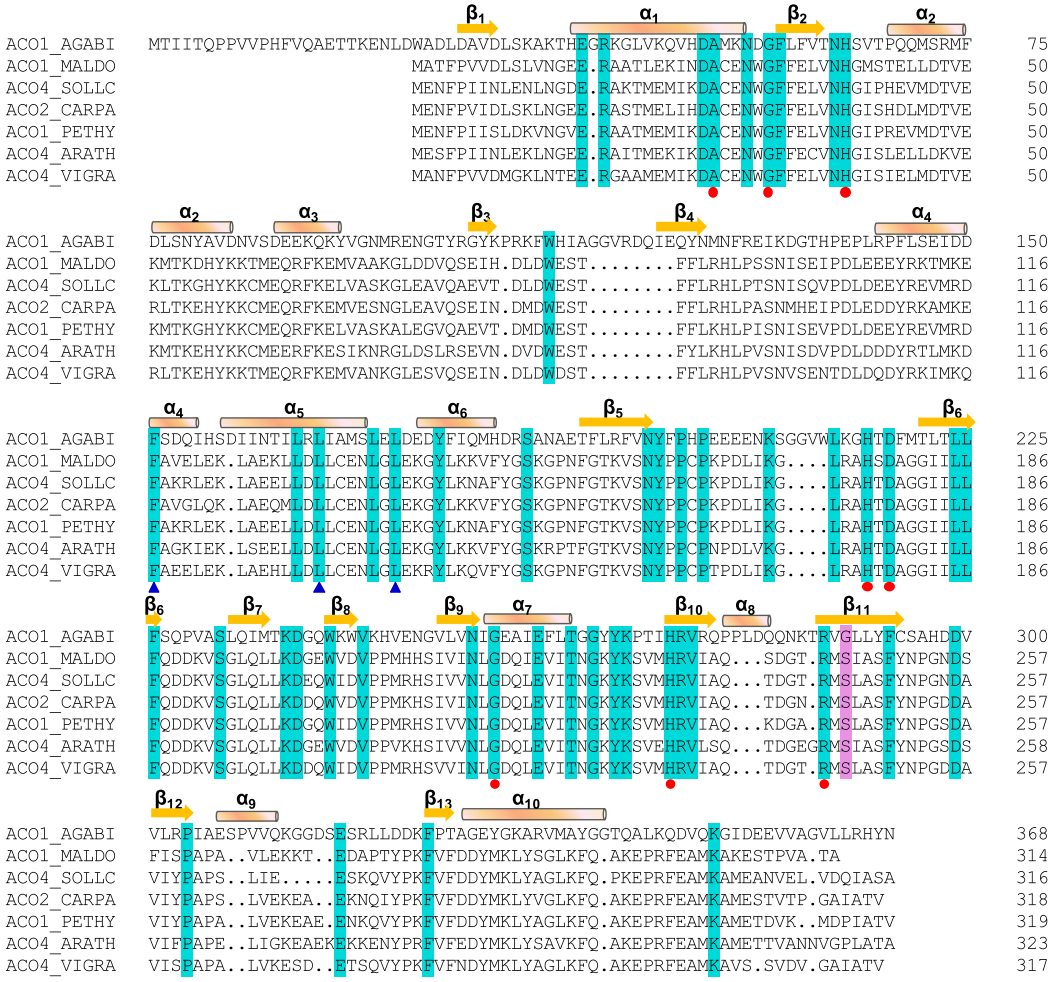

Fig. 1. Sequence alignment of several ACC oxidases (ACOs). Shown are sequences of ACO1_AGABI from *A. bisporus* (SWISSPROT H9ZYN5), ACO1_MALDO from *M. domestica* (SWISSPROT Q00985), ACO4_SOLLC from *S. lycopersicum* (SWISSPROT P24157), ACO2_CARPA from *C. papaya* (SWISSPROT Q9ZRC9), ACO1-PETHY from *P. hybrida* (SWISSPROT Q08506), ACO4_ARATH from *A. thaliana* (SWISSPROT Q06588), and ACO_VIGRA from *V. radiata* (SWISSPROT Q2KTE3). Amino acid residues conserved throughout the seven enzymes are highlighted in cyan and residues marked with blue triangles form a potential leucine zipper. Eight conserved amino acid residues of Fe (II) ascorbate family of dioxygenases are denoted by red dots. A putative active site residue different from plant ACOs is highlighted in magenta. The secondary structures shown above the sequences are as assigned for ACO from *A. bisporus*. Helices are shown in light orange and strands are in yellow.

respectively (Fig. 3). The tertiary mutant H216D/D218E/H273Q did not completely lose catalytic activity, which was different from the results of plant ACOs [38,39]. These results could be due to the incomplete disruption of the hydrogen bonds by the point mutation.

On the inner face of the active site, the residues are mostly conserved as identical or similar residues compared to plant ACOs (Fig. 2B, C) [27,36]. However, a key active site residue belonging to the conserved RXS motif, S289, which is an important catalytic residue in plant ACOs, is replaced by G289 (Fig. 2C, D). It has been widely speculated that both ascorbate and bicarbonate are essential for plant ACO activity [36,38], and the latter might be secured in the ACO active site through interaction with R and S residues of the RXS motif. Thus, we performed site-directed mutagenesis to substitute the R287 and G289 residues by glycine and serine residues, respectively, to investigate whether the RXS motif is essential for the activity of Ab-ACO. The results showed that the ACO activity of R287G was remarkably decreased to nearly 40% compared to the wild-type, proving that R287 played an important role for enzyme activity (Fig. 3). Strikingly, the enzyme activity of G289S was three times as high as that of the wild type (Fig. 3), clearly demonstrating the importance of the integrity of the RXS motif for Ab-ACO activity. Additionally, these results gave a comparatively proper explanation for the relatively low catalytic activity compared with plant ACOs.

3.4. Biochemical and kinetic properties

The steady-state kinetic parameters of the recombinant Ab-ACO protein were determined at pH 7.2 (in Tris–HCl buffer), 30 °C. In terms of the calculation of the K_m of Ab-ACO, the activity of Ab-ACO approached saturation at an ACC concentration of 0.5 mM (Fig. 4A). The apparent K_m for ACC determined from the Lineweaver–Burk plot was 0.25 mM, which is similar to 0.24 mM K_m^{ACC} for MD-ACO [40] but contrasts with 36 μM K_m^{ACC} for avocado [41]. Although Ab-ACO was capable of catalysing ethylene formation in the absence of Fe^{2+}, the activity was 2.4-fold lower than that in the steady-state reaction when 2.5 μM Fe^{2+} was added (Fig. 4B). The maximal activity was obtained when the Fe^{2+} concentration reached 10 μM, and the apparent $K_m^{Fe(II)}$ was 1.25 μM. Fig. 4C showed that ethylene was produced when Ab-ACO was combined with ACC and Fe^{2+} in the presence of $NaHCO_3$, but in the absence of ascorbate. Hence, ascorbate is not required for ethylene production. The optimal concentration of ascorbate for Ab-ACO (1 mM) was dramatically lower when compared with that required for recombinant MD-ACOs (20–30 mM) [40]. Interestingly, Ab-ACO activity declined as ascorbate concentration increased, which was consistent with MD-ACOs expressed in *E. coli* [40] and LE-ACOs expressed in yeast [42].

CO_2 is a necessary activator for plant ACO reactivity both in vivo and in vitro [1,16]. In this study, Ab-ACO activity was completely abolished

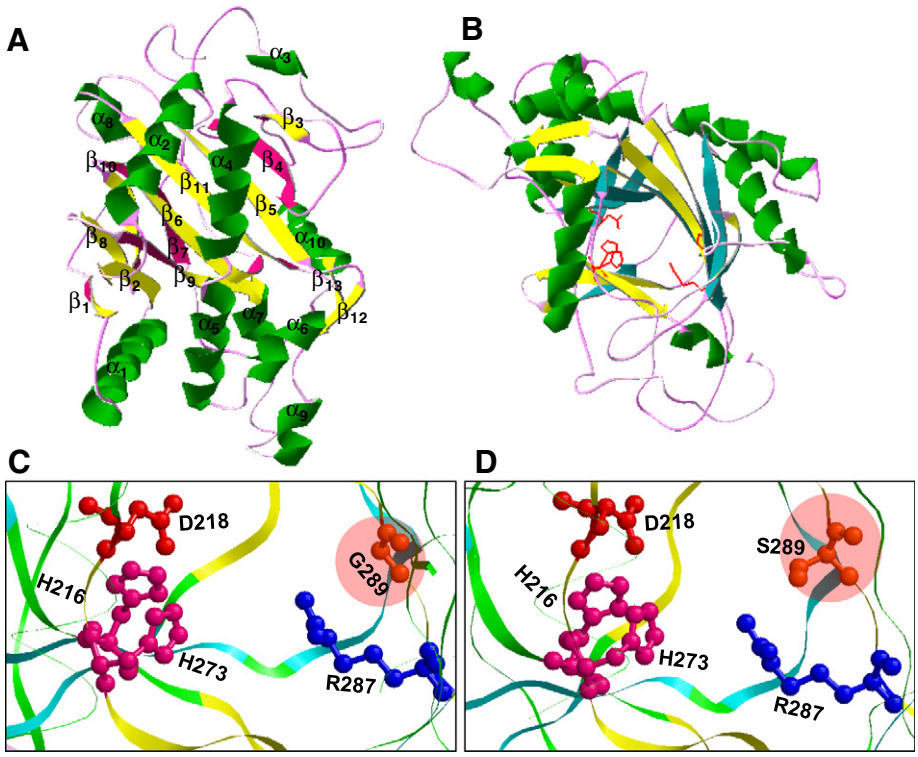

Fig. 2. Structural model of 3D fold of Ab-ACO obtained using homology modelling approach based on the crystal structure of protein ANS structure from *A. thaliana* (PDB code 1GP6) as a template. (A) 3D structure of Ab-ACO was drawn in ribbon plot. Secondary-structural elements are annotated: the α helices are shown in green, and the β strands are in purple and yellow; (B) Stereo view of the overall structure. Important active site residues, H216, D218, H273, R287 and G289, are shown in red; (C) and (D) Close-up of the active site region of the wild type Ab-ACO and the G289S mutant. Side chains of key residues are represented as ball and stick models. The side chains of the five putative conserved active site residues, H216, D218, H273 and R287, G289/S289, are displayed in magenta, red, magenta, blue and orange, respectively.

in the absence of $NaHCO_3$, and no ethylene was produced (Fig. 5), suggesting that $NaHCO_3$ has an essential role. In the absence of bicarbonate, avocado ACO was also unable to efficiently oxidise ACC to ethylene; however, the ferrous ion was still oxidised to the ferric state [43], which reflected "incorrect" binding of ACC and/or dioxygen. It has been reported that the R244K mutation in tomato pTOM13 ACO caused the enzyme to require 5-fold more bicarbonate than the wild-type for optimal activity, and the activity of the R244K mutant increased 17-fold in the presence of 50 mM bicarbonate relative to that without added bicarbonate [36]. Similarly, the activity of the R287G mutant decreased to 1.73–2.30 times lower than that of the wild type at the same level of bicarbonate (Fig. 5). Consequently, R287G required 4–5-fold more bicarbonate than the wild-type for similar activity. In addition, the R289S mutation dramatically reduced the bicarbonate dependence, with $K_m^{NaHCO_3}$ decreasing from 58.17 ± 4.95 in the wild-type to 25.33 ± 3.34 in the G289S (Fig. 5B). These results indicate the probable involvement of R287 and S289 in direct or indirect binding with bicarbonate, resulting in putative conformational changes in the active site of the enzyme.

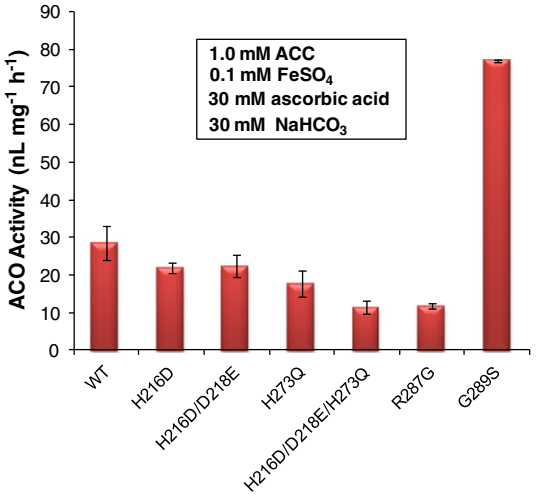

Fig. 3. Specific activities of the wild-type and mutant Ab-ACO enzymes. The recombinant enzyme activity was measured under standard reaction conditions (100 mM Tris–HCl buffer, pH 7.2, containing 1.0 mM ACC, 30 mM ascorbic acid, 0.1 mM $FeSO_4$, 30 mM $NaHCO_3$ and 0.067 mg of purified enzyme in a final volume of 2.5 mL at 30 °C). The H216D/D218E mutant was mutated at both H216 and D218 residues, and the H216D/D218E/H273Q mutant was mutated at H216, D218, and H273 residues. The results are means ± SD of three repeated experiments.

3.5. Determination of Fe^{2+} binding affinities by spectral measurements

The differences of the site-mutagenesis data on Fe^{2+}-binding residues between Ab-ACO and plant ACOs led us to further study the effect of Fe^{2+}-binding on the conformation of Ab-ACO using fluorescence and CD spectroscopy. Intrinsic fluorescence of proteins is a powerful tool for monitoring the microenvironment of Trp residues in proteins [44]. This tool has been successfully used to study the binding of metals to several proteins [45], including tomato ACO [46] and an ACO-related enzyme, 2-OG-dependent dioxygenase TfdA [47]. Fig. 6A shows the changes in the fluorescence intensity upon Fe^{2+}-binding. The intrinsic fluorescence from Ab-ACO was characterised by an emission maximum (λ_{max}) band at approximately 340 nm (with λ_{ex} = 280 nm), indicating that most of the observed fluorescence was contributed by the tryptophan residue. As shown in Fig. 6A, an addition of 45 μM Fe^{2+} led to an approximately 60% decrease of fluorescence intensity with almost no shift in the λ_{max}, suggesting that Fe^{2+} caused a change in the local tertiary structure around the tryptophan residues in Ab-ACO. Moreover,

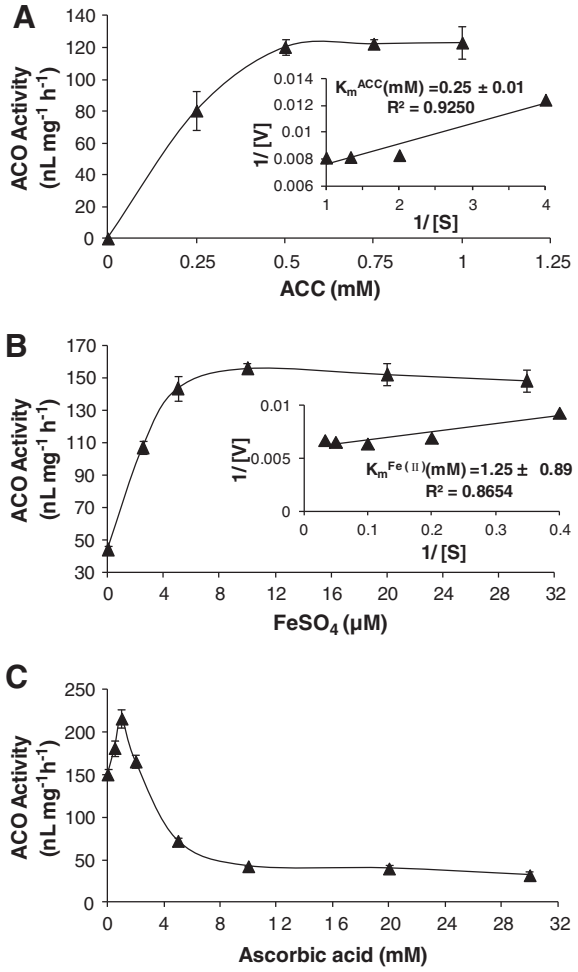

Fig. 4. Enzyme activities of Ab-ACO enzyme at different concentrations of substrates. The reactions were performed with systematically varied concentrations of ACC (A), $FeSO_4$ (B), and ascorbic acid (C). The concentrations of the constant substrates were maintained at 1.0 mM ACC, 0.1 mM $FeSO_4$, 2.0 mM ascorbic acid and 30 mM $NaHCO_3$. The inset of (A) and (B) corresponds to the Lineweaver–Burk plot of the enzyme activity versus concentration of ACC and $FeSO_4$, respectively, for calculating the kinetic constants. The values are derived from the means ± SD of three repeated experiments.

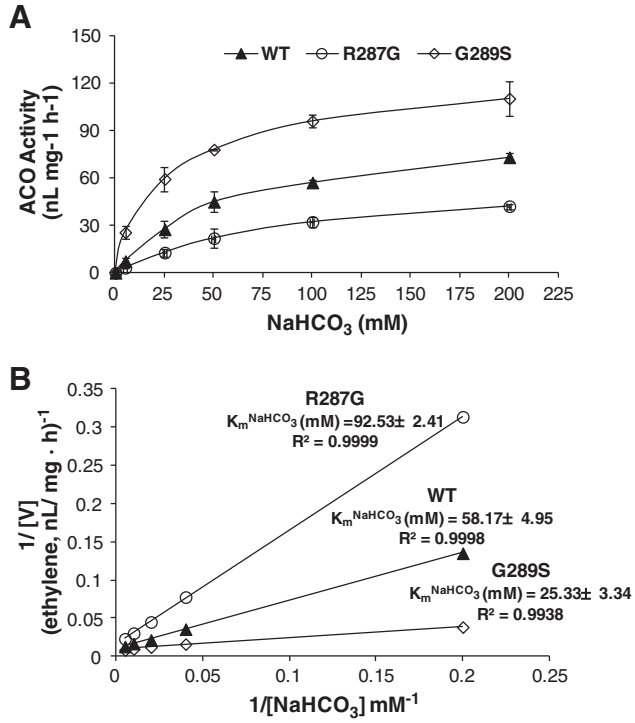

Fig. 5. Enzyme activities of the wild-type and mutant Ab-ACO enzymes in different concentrations of $NaHCO_3$ (A), and the corresponding Lineweaver–Burk (double reciprocal) plots (B). The reactions were performed under the conditions of 100 mM Tris–HCl buffer, pH 7.2, containing 1.0 mM ACC, 30 mM ascorbic acid and 0.1 mM $FeSO_4$ in a final volume of 2.5 mL. The values are derived from means ± SD of three repeated experiments.

the degree of change in fluorescence intensity was a function of the ferrous concentration (5–45 μM). The change was most likely attributed to the net exposure of aromatic residues to an aqueous environment upon the binding of the ferrous ion to the protein [48].

The H216D, H273Q, H216D/D218E and H216D/D218E/H273Q mutants each lack a residue or residues that function as ligands to the metal binding site, and the mutants might be expected to bind Fe^{2+} more weakly, but the fluorescence changes demonstrated this might not be correct. Fluorescence quenching was also strong when Fe^{2+} was added to all mutant forms of Ab-ACO, except for the tertiary mutant H216D/D218E/H273Q (Fig. S4). By contrast, H114A and D116A TfdA variants, lacking either a histidine or aspartic acid metallocentre ligand, exhibited weaker affinity for Fe^{2+} [47]. This result could also explain the incomplete inhibition of enzyme activity by point mutations on the Fe^{2+}-binding residues.

The structural changes of Ab-ACO upon Fe^{2+} binding were also monitored by far-UV CD spectroscopy (Fig. 6B). The addition of Fe^{2+} to the protein resulted in only a slight change in the CD spectrum, demonstrating that the presence of ferrous had no effect on the secondary structure of the protein. Thus, the ferrous ion was able to induce a change only in the tertiary structure of the protein, but not the secondary structure.

4. Discussion

ACC oxidase, along with ACC synthase, is a key regulatory enzyme for ethylene production in climacteric fruits, the biochemical mode and catalytic mechanism of plant ACOs have been investigated in detail [23,27,36,43,46]. Turner et al. [12] and Ward et al. [13] have shown that *A. bisporus* also produces ethylene. *A. bisporus* is the most cultivated edible mushroom worldwide and has nutritional and medicinal value [14,49]. Compared with the plant counterpart, however, ethylene released from edible mushrooms has received little attention. This may be because ethylene is a naturally produced growth regulator in higher plants while the regulatory role of ethylene in the growth or development of edible mushrooms remains unclear. Our research focuses on ACC oxidase in the edible mushrooms *A. bisporus*. This is the first report of an ethylene-forming enzyme specifically expressed in edible mushrooms.

In this study, we isolated and identified an ACC oxidase homologue gene from *A. bisporus* that was recombinant expressed in *E. coli* and purified to homogeneity as indicated by SDS-PAGE results (Fig. S1) and a single N-terminal amino acid sequence. The molecular weight of this protein was ~42 kDa, which was close to the size range (35–41 kD) reported for ACC oxidase proteins from plant species [16,50,51] and the slime mould *Dictyostelium discoideum* (42.9 kDa) [10]. The amino acid sequence of this putative ACC oxidase Ab-ACO (368 amino acids) was deduced from the nucleotide sequences and this protein only shares 20.9%–22.8% of identity and 38.1%–40.5% of similarity with higher plant ACOs (Fig. 1). However, Ab-ACO was found to contain a conserved 2-oxoglutalate (2OG) and Fe (II) dependent oxygenase superfamily domain (201–296th amino acids from the initiation site) [52], which is the characteristic of enzymes that catalyse the oxidation of the organic substrates such as ACC, and two histidine sites at positions 216 and 273 for binding iron which are necessary for the activation of the enzyme (Fig. 1). According to the alignment among known ACC

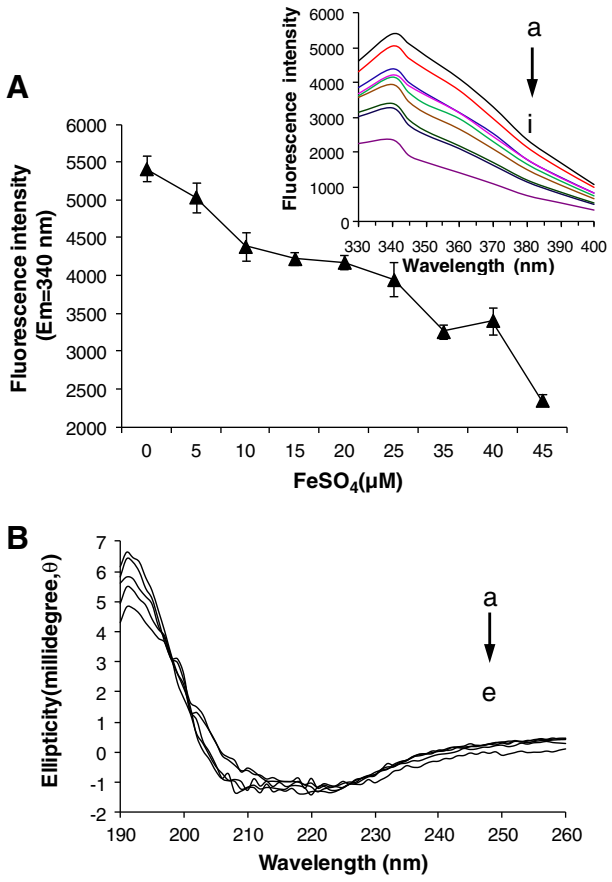

Fig. 6. Fluorescence and far-UV CD spectral studies of Ab-ACO as a function of increasing free Fe^{2+} concentrations. (A) The changes in the fluorescence spectral intensity at 340 nm of the Ab-ACO. The inset of (A): the fluorescence spectral intensity of the Ab-ACO produced by various concentrations of Fe^{2+} (a, 0 μM; b, 5 μM; c, 10 μM; d, 15 μM; e, 20 μM; f, 25 μM; g, 35 μM; h, 40 μM; i, 45 μM). The protein sample was excited at 280 nm. Emission scans were from 330 nm to 400 nm; (B) The far-UV CD spectra of the Ab-ACO produced by various concentrations of Fe^{2+} (a, 0 μM; b, 3 μM; c, 30 μM; d, 300 μM; e, 1000 μM). All of the experiments were performed in triplicate. The solution contained 0.15 mg/mL proteins in 50 mM Tris—HCl buffer, pH 7.2.

oxidases, eight of the twelve amino acid residues conserved among all members of a superfamily that requires Fe (II) and ascorbate for activity [33] can be found in the sequence of Ab-ACO. The 1st (P29), 7th (L234), 8th (Q235) and 12th (S289) conserved amino acids have been replaced by aspartic acid, glutamine, isoleucine and glycine, respectively, in Ab-ACO, which indicates that these four conserved amino acids are not absolutely required for Ab-ACO activity (Figs. 3–5). However, the common Fe^{2+}-binding motif (H-X-D-X (54)-H) and the putative co-substrate hydrogen-binding residue (R287) which belongs to the RXS motif are well conserved in Ab-ACO (Fig. 1) as in other members in the non-heme iron enzyme family [23].

Plant ACC oxidase is well known for requiring Fe (II) and ascorbate to catalyse ACC in the presence of O_2 into ethylene, CO_2, HCN, dehydroascorbate, and two molecules of water. Furthermore, the activity of ACC oxidase is activated by CO_2 (or bicarbonate, HCO_3) [16]. These peculiarities have inspired many investigations on the structure–function relationships of ACO to shed light on the catalytic roles of Fe (II), ascorbate and bicarbonate. The crystal structure of ACO from *P. hybrida* (PDB ID: 1WA6) has been solved, but with no data on the binding of the different cofactors at the active site. This protein presents a conserved jelly-roll motif composed of β-strands harbouring the active site of the enzyme. No active site divergence has been observed in the corresponding putative β-strands of Ab-ACO, except for the replacement of a serine residue by a glycine residue on β-strand 11 (Fig. 2). Putative metal ligand amino acids H216 and H273 and D218 [53] are also present within the active site of the Ab-ACO. R287, which has been suggested to be involved in generating the reaction product during enzyme catalysis [27], is conserved and points towards the core. The abovementioned features raise the question of whether the differences in the protein sequences and structures reflect differences in the enzyme properties. Here, we demonstrated that Ab-ACO was successfully synthesised in a prokaryotic expression system with the enzymatic ability to convert ACC to ethylene (Fig. 3). The purified recombinant Ab-ACO had a specific activity of 28.6 nL mg^{-1} h^{-1}, which is significantly lower than the value of 1300 nL mg^{-1} h^{-1} for apple ACC oxidase expressed in *E. coli* [27] and the values of 66–550 nL mg^{-1} h^{-1} for tomato ACOs expressed in yeast [42]. This differential activity might be explained by incorrect folding or lower stability in the *E. coli* expression system, but this activity could also be a result of the intrinsic properties of the mushroom and plant enzymes or from variable amounts of ACC and co-substrates in the reaction medium. The mutagenesis data strongly supported the idea that the different residues in the protein active site, especially the absence of serine at residue 289, could account for the low activity (Fig. 3). This observation is inconsistent with apple ACO1 [27] where the hydroxy group of the nearby S246 was not a major determinant of enzyme activity.

The biochemical properties of Ab-ACO and plant ACOs revealed few differences with regard to substrate and cofactor requirements. One common feature between Ab-ACO and plant ACOs was the apparent K_m towards ACC. On the other hand, Ab-ACO also required the addition of Fe^{2+} for activity in vitro, and $NaHCO_3$ was absolutely required for activity in vitro. Foremost among these similarities was the putative involvement of R287 in bicarbonate binding to activate ACO reactivity, which agreed with the results of tomato ACO reported by Zhang et al. [36]. In contrast, several results obtained from mutagenesis studies have suggested that the side chain of R244 is critical for establishing a hydrogen-bonding network between apple ACO1 and the ascorbate molecule, indicating the participation of R244 in the ascorbate binding [23,27]. The absence of marked differences in the biochemical properties is not surprising given the little divergence of amino acids in the putative active site of the enzyme (Figs. 1–2). In comparison, Ab-ACO had two features that differ from plant ACOs. One significant difference is that ascorbate is not required in Ab-ACO for product formation. This result was contradictory to the previous conclusions that ACO activity was absolutely dependent upon the presence of ascorbate [16,40,42]. Rocklin et al. [43] reported that ascorbate was not required to activate avocado ACO for ACC oxidation to form ethylene. However, ascorbate was the best reductant for the steady-state reaction and was an efficient effector to accelerate the reaction. Another important observation was that the substitution of glycine for serine at residue 289 could be responsible not only for the low activity but also for the high demand on bicarbonate of Ab-ACO (Fig. 5). Rocklin et al. [43] suggested that bicarbonate might be secured in the ACO active site through interactions with the conserved RXS motif. In addition to this, ACC is stabilised by the bicarbonate cofactor, and any destabilisation of the bicarbonate binding would directly affect the efficiency of ACO [46]. Thus, we proposed that S246 could be involved in bicarbonate binding.

Although Ab-ACO and plant ACOs have a similar metal binding structural motif to anchor a ferrous ion in the active site, Ab-ACO surprisingly displayed different behaviours. All of the mutants of the Fe (II)-binding sites (H216, D218 and H273) of Ab-ACO still retained 40–78% of the wild-type enzyme activity, whereas an apparent complete loss of activity was observed in the apple ACC oxidase mutants when H177, D179 and H234 were substituted with various amino acids [39]. To obtain a better insight into the interaction of the Fe^{2+} at the active site, the experiments of tryptophan fluorescence quenching and CD spectroscopy were carried out. Binding of Fe^{2+} to the protein had little effect on the secondary structure of the protein (Fig. 6B), but Fe^{2+} binding induced a change in the tertiary structure of Ab-ACO (Fig. 6A). These results are similar to those reported for tomato ACO [46]. Lehrer [54] and Horrocks [55] proposed that the mechanism of

fluorescence quenching upon metal binding is a long-range energy transfer to an absorption band produced by the metal–protein interaction, which leads to a significant loss of emission intensity. Although all of the five tryptophan residues (W25, W112, W212, W242 and W244) in Ab-ACO are located relatively far (distances ranging from 8 to 21 Å) from the conserved Fe^{2+}-binding residues in the active site, the tryptophan fluorescence quenching upon iron binding was strong. Additions of 45 μM Fe^{2+} led to an ~60% decrease of fluorescence intensity, which is comparable to the results in tomato ACO and TfdA (~80% reduction) [46,47]. The data showed that Ab-ACO protein should have a motif for Fe^{2+} binding. This motif, inferred from the sequence and structure analysis, may be similar to the motif found in plant ACOs. Although the fluorescence quenching was also strong when Fe^{2+} was added to the one or the double mutants of the three putative iron coordinators, there was very little change for the tertiary mutant H216D/D218E/H273Q (Fig. S4). This result indirectly supports the idea that two histidines and a carboxylate group occupy the three vertices of the iron octahedral coordination in Ab-ACO.

It is reasonable to believe that *A. bisporus* is able to produce ethylene through a pathway similar to that of higher plants, although there are differences in the biochemical and catalytic characteristics of the enzymes (ACC oxidase). The pathway of ethylene production differs from the pathways identified in other fungi, such as *Botrytis cinerea* [4] and *Cryptococcus albidus* [7]. In contrast, ethylene in the slime mould *D. mucoroide* was demonstrated to be synthesised from methionine through SAM and ACC [10], as is the case of higher plants. It is easy to conclude that several ethylene biosynthesis pathways may coexist in the same species judging from an evolutional point of view. Philip [56] argued that the acquisition of the ACC oxidase was a crucial evolutionary step in the development of an ethylene biosynthesis pathway. Before ACC became the precursor for ethylene formation, ethylene may have been synthesised and accumulated in response to a pathogen attack. Thus, the present findings not only provide a supplement or an alternative pathway for ethylene biosynthesis in fungi but also enhance the previous understanding in this research area.

In closing, the present work suggests for the first time that *A. bisporus* is capable of catalysing ethylene production by ACC oxidase, which is the first protein shown to convert ACC to ethylene in edible mushrooms. In contrast to plant ACOs, Ab-ACO exhibits relatively low activity but similar conserved residues in the active site, except for the absence of S289. The kinetic properties of Ab-ACO did not markedly differ from the kinetic properties of plant ACOs in terms of co-factors and co-substrate requirements. However, ascorbate was not required for ethylene formation. The replacement of S289 by G289 is proposed to be responsible for the low catalytic activity and the high demand for bicarbonate. Moreover, the binding ferrous ion has a great effect on the tertiary structure of the protein. All of these results not only contribute to understanding the ethylene biosynthesis in fungi but also promote researches of the role of ethylene in the regulation of mushroom growth and development.

Acknowledgements

This project was supported by the Basic Research funds in Renmin University of China from the Central Government (13XNLI01).

Appendix A. Supplementary data

Supplementary data to this article can be found online at http://dx.doi.org/10.1016/j.bbagen.2013.08.030.

References

[1] S.F. Yang, N.E. Hoffman, Ethylene biosynthesis and its regulation in higher plants, Annu. Rev. Plant Physiol. 35 (1984) 155–189.
[2] L. Ilag, R.W. Curtis, Production of ethylene by fungi, Science 159 (1968) 1357–1358.
[3] J.M. Lynch, Identification of substrates and isolation of microorganism responsible for ethylene production in the soil, Nature 240 (1972) 45–46.
[4] S.M. Cristescu, D. De Martinis, S.L. Hekkert, D.H. Parker, F.J.M. Harren, Ethylene production by *Botrytis cinerea* in vitro and in tomatoes, Appl. Environ. Microbiol. 68 (2002) 5342–5350.
[5] D.O. Adam, S.F. Yang, Ethylene biosynthesis: identification of ACC as an intermediate in the conversion of methionine to ethylene, Proc. Natl. Acad. Sci. U. S. A. 76 (1979) 170–174.
[6] R. Fluhr, A.K. Mattoo, Ethylene-biosynthesis and perception, Crit. Rev. Plant Sci. 15 (1996) 479–523.
[7] H. Fukuda, M. Takahashi, T. Fujii, M. Tazaki, T. Ogawa, An NADH:Fe(III)EDTA oxidoreductase from *Cryptococcus albidus*: an enzyme involved in ethylene production in vivo? FEMS (Fed. Eur. Microbiol. Soc.) Microbiol. Lett. 60 (1989) 107–111.
[8] K. Nagahama, T. Ogawa, T. Fujii, M. Tazaki, S. Tanase, Y. Morino, H. Fukuda, Purification and properties of ethylene-forming enzyme from *Pseudomonas syringae* pv. *phaseolicola* PK2, J. Gen. Microbiol. 137 (1991) 2281–2286.
[9] B. Völksh, H. Weingart, Comparison of ethylene-producing *Pseudomonas syringae* strains isolated from kudzu (*Pueraria lobata*) with *Pseudomonas syringae* pv. *phaseolicola* and *Pseudomonas syringae* pv. *glycinea*, Eur. J. Plant Pathol. 103 (1997) 795–802.
[10] A. Amagai, Ethylene as a potent inducer of sexual development, Dev. Growth Differ. 53 (2011) 617–623.
[11] Y.J. Jia, Y. Kakuta, M. Sugawara, T. Igarashi, N. Oki, M. Kisaki, T. Shoji, Y. Kanetuna, T. Horita, H. Matsui, M. Honma, Synthesis and degradation of 1-aminocyclopropane-1carboxylic acid by *Penicillium citrinum*, Biosci. Biotechnol. Biochem. 63 (1999) 542–549.
[12] E.M. Turner, M. Wright, T. Ward, D.J. Osborne, R. Self, Production of ethylene and other volatiles and changes in cellulase and laccase during the life-cycle of the cultivated mushroom, *Agaricus bisporus*, J. Gen. Microbiol. 91 (1975) 167–176.
[13] T. Ward, E.M. Turner, D.J. Osborne, Evidence for the production of ethylene by the mycelium of *Agaricus bisporus* and its relationship to sporocarp development, J. Gen. Microbiol. 104 (1978) 23–30.
[14] E. Morina, A. Kohler, A.R. Baker, M. Foulongne-Oriol, V. Lombard, et al., Genome sequence of the button mushroom *Agaricus bisporus* reveals mechanisms governing adaptation to a humic-rich ecological niche, Proc. Natl. Acad. Sci. U. S. A. 109 (2012) 17501–17506.
[15] A.J. Hamilton, G.W. Lycett, D. Grierson, Antisense gene that inhibits synthesis of the hormone ethylene in transgenic plants, Nature 346 (1990) 284–287.
[16] J.G. Dong, J.C. Fernandez-Maculet, S.F. Yang, Purification and characterization of 1-aminocyclopropane-1-carboxylate oxidase from apple fruit, Proc. Natl. Acad. Sci. U. S. A. 89 (1992) 9789–9793.
[17] D.G. McRae, J.A. Coker, R.L. Legge, J.E. Thompson, CO_2 requirement for ACCO, Plant Physiol. 73 (1983) 784–790.
[18] G.D. Peiser, T.T. Wang, N.E. Hoffman, S.F. Yang, H.W. Liu, C.T. Walsh, Formation of cyanide from carbon 1 of 1-aminocyclopropane-1-carboxylic acid during its conversion to ethylene, Proc. Natl. Acad. Sci. U. S. A. 81 (1984) 3059–3063.
[19] E.I. Solomon, T.C. Brunold, M.I. Davis, J.N. Kemsley, S.K. Lee, N. Lehnert, F. Neese, A.J. Skulan, Y.S. Yang, J. Zhou, Geometric and electronic structure/function correlations in non-heme iron enzymes, Chem. Rev. 100 (2000) 273–278.
[20] D.M. Meng, L. Shen, X.H. Zhang, J.P. Sheng, Isolation of high quality and yield of RNA from *Agaricus bisporus* with a simple, inexpensive and reliable method, Biotechnol. Lett. 34 (2012) 1315–1320.
[21] D.Y. Zhao, L. Shen, B. Fan, M.M. Yu, Y. Zheng, S.N. Lv, J.P. Sheng, Ethylene and cold participate in the regulation of *LeCBF1* gene expression in postharvest tomato fruits, FEBS Lett. 583 (2009) 3329–3334.
[22] B.L. Wang, Y. Xu, C.Q. Wu, Y.M. Xu, H.H. Wang, Cloning, expression, and refolding of a secretory protein ESAT-6 of *Mycobacterium tuberculosis*, Protein Expr. Purif. 39 (2005) 184–188.
[23] A. Yoo, Y.S. Seo, J.W. Jung, S.K. Sung, W.T. Kim, W. Lee, D.R. Yang, Lys296 and Arg299 residues in the C-terminus of MD-ACO1 are essential for a 1-aminocyclopropane-1-carboxylate oxidase enzyme activity, J. Struct. Biol. 156 (2006) 407–420.
[24] M.M. Bradford, A rapid and sensitive method for the quantitation of microgram quantities of protein utilizing the principle of protein-dye binding, Anal. Biochem. 72 (1976) 248–254.
[25] M.L. Li, S.J. Yun, X.L. Yang, G.H. Zhao, Stability and iron oxidation properties of a novel homopolymeric plant ferritin from adzuki bean seeds: a comparative analysis with recombinant soybean seed H-1 chain ferritin, Biochim. Biophys. Acta 1830 (2013) 2946–2953.
[26] L.A. Kelley, M.J.E. Sternberg, Protein structure prediction on the web: a case study using the Phyre server, Nat. Protoc. 4 (2009) 363–371.
[27] Y.S. Seo, A. Yoo, J.W. Jung, S.K. Sung, D.R. Yang, W.T. Kim, W. Lee, The active site and substrate-binding mode of 1-aminocyclopropane-1-carboxylate oxidase determined by site-directed mutagenesis and comparative modeling studies, Biochem. J. 380 (2004) 339–346.
[28] R.A. Laskowski, M.W. MacArthur, D.S. Moss, J.M. Thornton, PROCHECK: a program to check the stereochemical quality of protein structures, J. Appl. Crystallogr. 26 (1993) 283–291.
[29] D. Eisenberg, R. Lüthy, J.U. Bowie, VERIFY3D: assessment of protein models with three-dimensional profiles, Methods Enzymol. 277 (1997) 396–404.
[30] M.M. Yu, L. Shen, A.J. Zhang, J.P. Sheng, Methyl jasmonate-induced defense responses are associated with elevation of 1-aminocyclopropane-1-carboxylate oxidase in *Lycopersicon esculentum* fruit, J. Plant Physiol. 168 (2011) 1820–1827.
[31] J. Buchner, R. Rudolph, Renaturation, purification and characterization of recombinant Fab-fragments produced in *Escherichia coil*, J. Biotechnol. 9 (1991) 157–162.

[32] T. Kiefhaber, P. Rudolph, H.H. Kohler, J. Buchner, Protein aggregation in vitro and in vivo: a quantitative model of the kinetic competition between folding and aggregation, J. Biotechnol. 9 (1991) 825–829.
[33] T.I. Zarembinski, A. Theologis, Ethylene biosynthesis and action: a case of conservation, Plant Mol. Biol. 26 (1994) 1579–1597.
[34] J. Matsuda, S. Okabe, T. Hashimoto, Y. Yamada, Molecular cloning of hyoscyamine 6β-hydroxylase, a 2-oxoglutarate-dependent dioxygenase, from cultured roots of *Hyoscyamus niger*, J. Biol. Chem. 266 (1991) 9460–9464.
[35] H. Kende, Ethylene biosynthesis, Annu. Rev. Plant Physiol. Plant Mol. Biol. 44 (1993) 283–307.
[36] Z.H. Zhang, J.S. Ren, I.J. Clifton, C.J. Schofield, Crystal structure and mechanistic implications of 1-aminocyclopropane-1-carboxylic acid oxidase—the ethylene-forming enzyme, Chem. Biol. 11 (2004) 1383–1394.
[37] R.C. Wilmouth, J.J. Turnbull, R.W.D. Welford, I.J. Clifton, A.G. Prescott, C.J. Schofield, Structure and mechanism of anthocyanidin synthase from *Arabidopsis thaliana*, Structure 10 (2002) 93–103.
[38] V.J. Lay, A.G. Presott, P.G. Thomas, P. John, Heterologous expression and site-directed mutagenesis of the 1-aminocyclopropane-1-carboxylate oxidase from kiwi fruit, Eur. J. Biochem. 242 (1996) 228–234.
[39] J.F. Shaw, Y.S. Chou, R.C. Chang, S.Y. Yang, Characterization of the ferrous ion binding sites of apple 1-aminocyclopropane-1-carboxylate oxidase by site-directed mutagenesis, Biochem. Biophys. Res. Commun. 225 (1996) 697–700.
[40] J.E. Binnie, M.T. McManus, Characterization of the 1-aminocyclopropane-1-carboxylic acid (ACC) oxidase multigene family of *Malus domestica* Borkh, Phytochemistry 70 (2009) 348–360.
[41] J. McGarvey, H. Yu, R.E. Christoffersen, Nucleotide sequence of a ripening-related cDNA from avocado fruit, Plant Mol. Biol. 15 (1990) 165–167.
[42] S. Bidonde, M.A. Ferrer, H. Zegzouti, S. Ramassamy, A. Latché, J.C. Pech, A.J. Hamilton, D. Grierson, M. Bouzayen, Expression and characterization of three tomato 1-aminocyclopropane-1-carboxylate oxidase cDNAs in yeast, Eur. J. Biochem. 253 (1998) 20–26.
[43] A.M. Rocklin, K. Kato, H.W. Liu, L. Que Jr., J.D. Lipscomb, Mechanistic studies of 1-aminocyclopropane-1-carboxylic acid oxidase: single turnover reaction, J. Biol. Inorg. Chem. 9 (2004) 171–182.
[44] M.K. Jobby, Y. Sharma, Calcium-binding to lens βB2- and βA3-crystallINS suggests that all β-crystallINS are calcium-binding proteins, FEBS J. 274 (2007) 4135–4147.
[45] H.R. Lucas, J.C. Lee, Effect of dioxygen on copper (II) binding to alpha-synuclein, J. Inorg. Biochem. 104 (2010) 245–249.
[46] L. Brisson, N. El Bakkali-Taheri, M. Giorgi, A. Fadel, J. Kaizer, M. Réglier, T. Tron, El H. Ajandouz, A.J. Simaan, 1-Aminocyclopropane-1-carboxylic acid oxidase: insight into cofactor binding from experimental and theoretical studies, J. Biol. Inorg. Chem. 17 (2012) 939–949.
[47] J.C.D. Hotopp, T.A. Auchtung, D.A. Hogan, R.P. Hausinger, Intrinsic tryptophan fluorescence as a probe of metal and alpha-ketoglutarate binding to TfdA, a mononuclear non-heme iron dioxygenase, J. Inorg. Biochem. 93 (2003) 66–70.
[48] D. Lebeche, B. Kaminer, Characterization of a calsequestrin-like protein from sea-urchin eggs, Biochem. J. 287 (1992) 741–747.
[49] P. Manzi, A. Aguzzi, L. Pizzoferrato, Nutrition value of mushrooms widely consumed in Italy, Food Chem. 73 (2001) 321–325.
[50] E. Dupille, C. Rombaldi, J.M. Lelievre, J.C. Cleyet-Marel, J.C. Pech, A. Latche, Purification, properties and partial amino-acid sequence of 1-aminocyclopropane-1-carboxylic acid oxidase from apple fruits, Planta 190 (1993) 65–70.
[51] M.C. Pirrung, L.M. Kaiser, J. Chen, Purification and properties of the apple fruit ethylene-forming enzyme, Biochem. J. 32 (1993) 7445–7450.
[52] L. Aravind, E.V. Koonin, The DNA-repair protein AlkB, EGL-9, and leprecan define new families of 2-oxoglutarete- and iron-dependent dioxygenases, Genome Biol. 2 (2001)(research0007.1-research0007.8).
[53] P.L. Roach, I.J. Clifton, V. Fülöp, K. Harlos, G.J. Barton, J. Hajdu, I. Andersson, C.J. Schofield, J.E. Baldwin, Crystal structure of isopenicillin-N-synthase is the first from a new structural family of enzymes, Nature 375 (1995) 700–704.
[54] S.S. Lehrer, Fluorescence and absorption studies of binding of copper and iron to transferrin, J. Biol. Chem. 244 (1969) 3613–3617.
[55] W.D.W. Horrocks, Luminescence spectroscopy, Methods Enzymol. 226 (1993) 495–538.
[56] J. Philip, Ethylene biosynthesis: the role of 1-aminocyclopropane-l-carboxylate (ACC) oxidase, and its possible evolutionary origin, Physiol. Plant. 100 (1992) 583–592.